Journal of Manufacturing Processes 100 (2023) 91–98

Contents lists available at ScienceDirect

Journal of Manufacturing Processes

journal homepage: www.elsevier.com/locate/manpro

Generation of periodic nanobumps through a double-scan method with femtosecond lasers☆

Kewei Li, Shreyas Limaye, Xin Zhao *

Department of Mechanical Engineering, Clemson University, Clemson, SC 29634-0921, USA

ARTICLE INFO

Keywords:
Ultrafast laser surface structuring
Color effect
Nanobump
Double-scan
Polarization angle

ABSTRACT

Ultrafast laser surface structuring is a promising technique for precisely controlling the surface functions of materials. Nanoripples, the typical laser-induced periodic surface structures, are effective at regulating surface colors, but only in one view direction. To overcome this issue, effective methods for fabricating other types of structures are needed. In this study, we successfully form periodic nanobump structures using a simple double-scan approach, in which the same surface is subjected to two consecutive laser scans with different polarization directions. The formation behavior of these intriguing nanostructures is investigated in relation to laser parameters such as peak laser fluence, overlapping ratio, and polarization angle between two scans. The formation mechanism is hypothesized and confirmed. The obtained nanobumps exhibit exceptional optical performance compared to nanoripples by enhancing the visibility angle, hence expanding the possible applications of the ultrafast laser surface structuring technique.

1. Introduction

Inspired by fancy surface features in nature, such as the color effect of butterfly wings [1] and the self-cleaning function of lotus leaves [2], researchers have committed huge amounts of effort to fabricating artificial surface structures that replicate these surface functions. In recent decades, ultrafast laser surface structuring, also known as ultrafast laser texturing, has been shown to be an effective technique for processing solid surfaces with superior efficiency and precision [3–7]. Laser-induced periodic surface structures (LIPSSs), typically nanoripple structures, attract researchers' interest in exploring their promising application potential for customizing surfaces with superior surface wettability [8–10], optical [11–13], and mechanical [14,15] properties. Nanoripples are unidirectional structures whose alignment in metals [5] and dielectrics [10] is perpendicular and parallel to the laser polarization direction, respectively. Similar to nano-gratings, they are effective at regulating surface colors. However, due to its one-dimensional periodicity, the nanoripple-induced surface coloration has a restricted viewing angle range. By viewing in the direction parallel to the ripples, the color effect will disappear. To expand the view angle, surface structures with multi-dimensional periodicities are strongly required.

So far, some experimental and numerical efforts have demonstrated the attainability of two-dimensional periodic nanobumps with triangle [16,17], hexagon [18,19], and square [20,21] geometries. One widely studied method is the double-pulse method, in which two laser pulses are delivered onto the same spot with a super-short (picosecond-nanosecond) interpulse time delay. The polarization direction of the second pulse is rotated away from that of the first pulse. Through this method, uniform formation of nanobumps can be achieved. Nevertheless, the formation window by this method is very narrow. More importantly, the double-pulse method requires high-precision control of the interpulse time delay. This increases the complexity and cost of the optical system, which hinders its industrial application potential. We proposed a simple alternative approach, the double-scan method, to address those issues [22]. This technique involves exposing the material to two consecutive laser scans with orthogonal polarization orientations. Unlike the double-pulse method, the time delay between two scans is flexible, making the setup and implementation of this method significantly simpler. Some other studies also adopted similar methods to create nanostructures on different materials [23–27]. However, the formation mechanism of nanobumps by this method is still in debate. Gregorčič et al. [23] regarded these nanobumps as the results of a dynamic self-organization process. Kobayashi et al. [24] attributed the formation behavior to laser-induced surface reorganization/reconstruction (without material

☆ 51st SME North American Manufacturing Research Conference (NAMRC 51, 2023).

* Corresponding author.
E-mail address: xzhao5@clemson.edu (X. Zhao).

https://doi.org/10.1016/j.jmapro.2023.05.020
Received 5 April 2023; Accepted 2 May 2023
Available online 16 May 2023

removal) rather than ablation. Liu et al. [26] claimed that high spatial frequency LIPSSs (HSFLs) created by the second scan clipped the pre-generated nanoripples and subsequently formed 2D dot-like structures. Moreover, systematic study and analysis of the double-scan method are still lacking.

In this study, the formation behavior of nanobumps is investigated using the double-scan approach. The effects of peak laser fluence, overlapping ratio, and polarization angle on nanobump formation are investigated. The formation mechanism is proposed and verified with experimental results. The applicable domain of the double-scan method is discussed in depth.

2. Experimental setup

2.1. Materials

All tested samples in this work are stainless steel (AISI 304, size of each sample: 25.4 mm × 12.7 mm × 2.3 mm) with a polished mirror-like surface. Before laser irradiation and characterization, all samples were cleaned in an ultrasonic washer with pure isopropyl alcohol (99.9 % purity) for 5 min.

2.2. Laser irradiation and characterization

A Yb: KGW femtosecond laser system (PHAROS by Light Conversion) was utilized to generate linearly polarized laser pulses. The laser beam is Gaussian-shaped, and its beam diameter ω_0 (at $1/e^2$ of the peak intensity) is 34 μm after focusing. The laser central wavelength is 1030 nm, the repetition rate (f) is 100 kHz, and the laser pulse duration is 165 fs. The experimental setup is displayed in Fig. 1. The two-dimensional uniform scan in which the pulse distance (d_p) and scan pitch (d_l) were set to be equal is achieved with a laser scan head (intelliSCAN by SCANLAB). The size of each processed region was 8.0 mm × 8.0 mm.

In this work, a double-scan method (Fig. 2) was applied to fabricate nanobumps. The scanning pattern remained identical between the first and the second scans. In the second scan, the polarization direction was rotated relative to the first scan by a certain angle, which is referred to as polarization angle (θ) in this study. The polarization direction was controlled through a half-wave plate. The influence of polarization angle, peak laser fluence, and overlapping ratio on surface morphology variation were investigated, as listed in Table 1. The peak laser fluence is defined as:

$$F_0 = \frac{8E_{pulse}}{\pi\omega_0^2} \tag{1}$$

where E_{pulse} represents the pulse energy. The overlapping ratio along the scanning path, defining the ratio of the overlapping length of two consecutive laser pulses to the laser beam diameter, is calculated as:

$$\varphi = \left(1 - \frac{v}{\omega_0 \times f}\right) \times 100\% \tag{2}$$

where v is the scanning speed. All experiments were conducted in an ambient environment.

After laser scanning, the scanning electron microscope (SEM, Hitachi Regulus 8230) was used to characterize the obtained surface morphology. The spatial periodicity of generated nanostructures were measured by Gwyddion [28] over SEM images. A camera-based surface color measurement system (Fig. 3) was developed to examine the surface coloration effect on the processed samples. In this work, the surface coloration effect is regarded as the nanoripples/nanobumps-induced diffraction phenomenon, which could be described by the diffraction equation [29]:

$$m\lambda = d(sin\alpha \times cos\varphi + sin\beta), \tag{3}$$

where λ is the light wavelength, d is the spatial periodicity of generated surface structures, and m is the order of diffraction, which is an integer value. The illumination angle, viewing angle and nanoripple orientation angle are represented by α, β and φ, respectively. In this work, the viewing angle β was maintained as 5° while illumination angle α and nanoripple orientation angle φ were varied to check the color effect.

3. Results and discussions

3.1. Formation of nanobumps

The viability of creating nanobumps using the double-scan method with a polarization angle is based on the hypotheses that (1) nanoripples can superimpose with other existing structures; and (2) nanoripples' orientation mainly depends on polarization direction (perpendicular for metals) rather than initial surface roughness. If they are true, the first and second scans will generate nanoripples with different orientations,

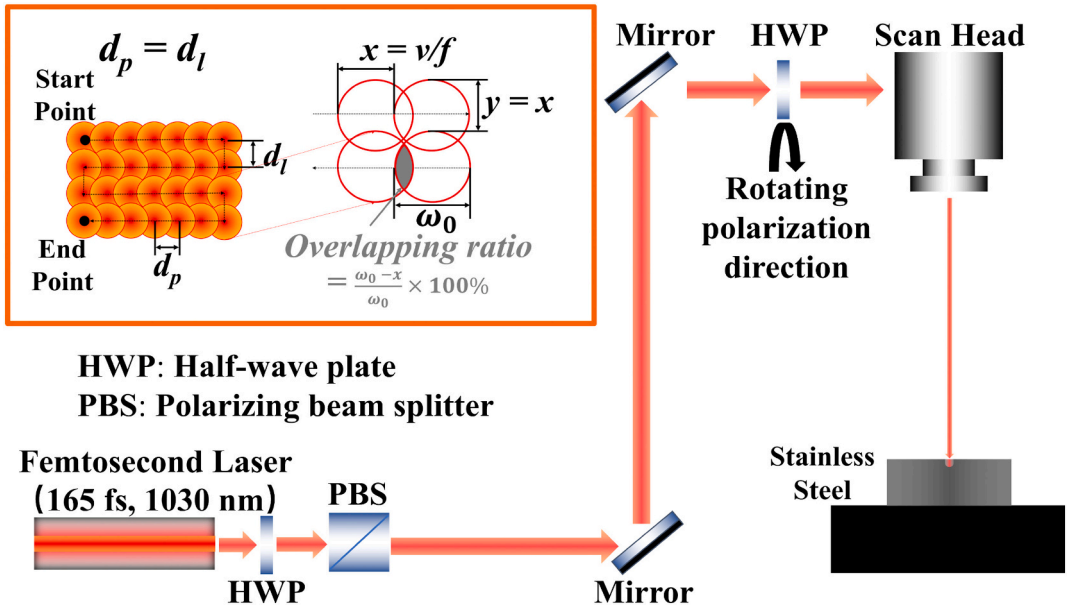

Fig. 1. Experimental setup and uniform scan strategy.

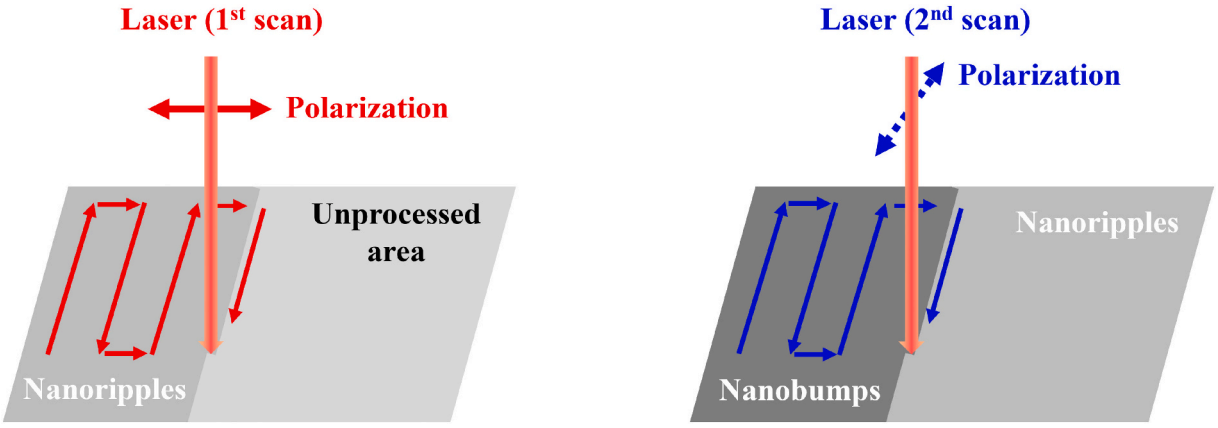

Fig. 2. Illustration of the double-scan method.

Table 1
Laser parameters.

Uniform scanning	First scan	Second scan
Repetition rate (kHz)	100	100
Laser fluence (J/cm^2)	2	0.1–0.8
Overlapping ratio (%)	75	40–95
Polarization angle (°)	–	0–90

which will interfere with each other and form nanobumps. Nanoripples are primarily referred to as low spatial frequency LIPSSs (LSFLs) in this work (Fig. 4(b)). By applying the double-scan method with carefully selected laser parameters (laser fluence is 2 J/cm^2 and 0.25 J/cm^2 for the first and second scan, respectively, and the overlapping ratio is kept at 75 %), periodic quasi-square-shaped nanobumps were successfully created, as shown in Fig. 4(c). These nanobumps structures align well in the horizontal direction and vertical direction, exhibiting two-dimensional periodicity as expected.

The coloration effects of the nanobumps and nanoripples were tested and compared in Fig. 4(d–g). The illumination angle α was set as 30° in Fig. 4(d) and (e). The top triangle in Fig. 4(d) is covered with nanoripples aligned horizontally, while the bottom triangle is covered with nanobumps. At this viewing angle ($\beta = 5°$) and nanoripple orientation angle ($\varphi = 0°$), both structures exhibit superior and comparable coloring effects. However, when the sample is rotated by 90° counterclockwise, turning φ to 90°, as shown in Fig. 4(e), no color effect is displayed in the nanoripple-covered triangle (left). This is because the view direction becomes parallel to the nanoripple orientation, thereby inhibiting the nanoripples' diffraction function. In contrast, the nanobump-covered triangle (right) retains its vivid color well, thanks to the two-dimensional periodicity of nanobumps. This clearly demonstrates the advantages of nanobump structures on broadening visible angles for surface coloration or other optical properties, which significantly expands its application potential, such as for optical storage and display. Fig. 4(f) and (g) depict the color effect of the same sample when illuminated from a different angle ($\alpha = 25°$). It demonstrates that the color can be altered depending on the direction of illumination and shows the superior color angle resolution of these surface structures.

3.2. Effects of laser fluence and overlapping ratio

The second scan's energy deposition is crucial for obtaining nanobumps. Peak laser fluence and overlapping ratio are two common laser parameters that influence the deposition of laser energy. It is essential to

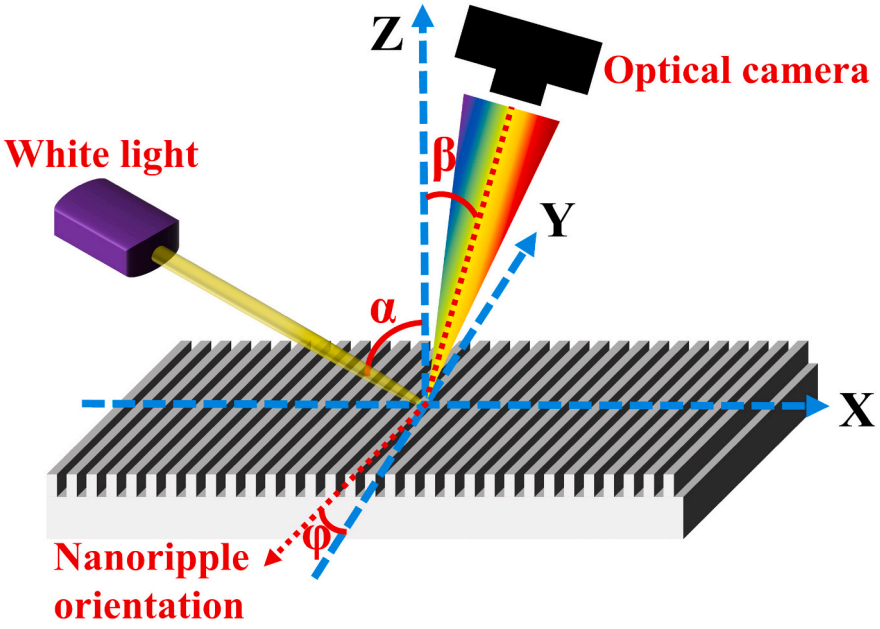

Fig. 3. Surface color measurement system.

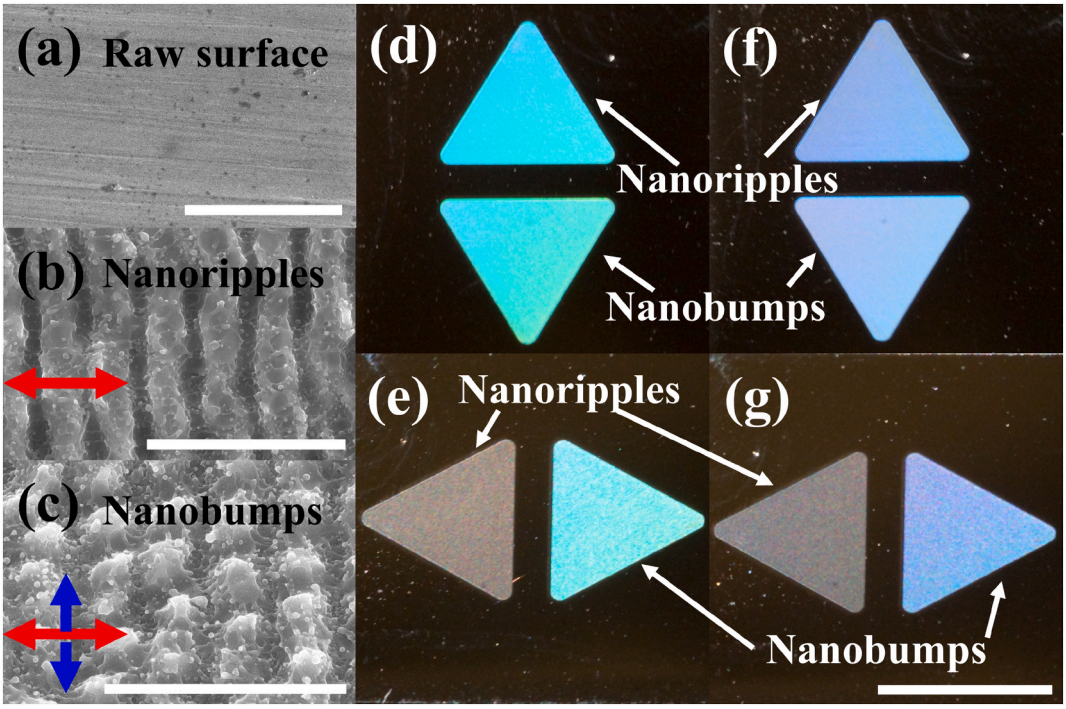

Fig. 4. SEM images of the raw surface (a), nanoripples obtained through one scan (b), and nanobumps generated by double-scan method (c), and their coloration effects at different illumination angles and nanoripple orientation angles (d–g). Red and blue double arrows in (b) and (c) indicate the polarization directions of the first and second scans, respectively. The scale bars are 3 μm (in (a–c)) and 3 mm (in (d–g)), respectively. (For interpretation of the references to color in this figure legend, the reader is referred to the web version of this article.)

examine their impact on the formation behavior of nanobumps. The effect of peak laser fluence of the second scan is revealed in Fig. 5. The first scan laser fluence was set to 2 J/cm^2, which is sufficient to produce regular nanoripples on the tested sample, shown in Fig. 4(b). The polarization directions between the first and second scans were orthogonal ($\theta = 90°$). After applying the second scan with 0.1 J/cm^2 laser fluence,

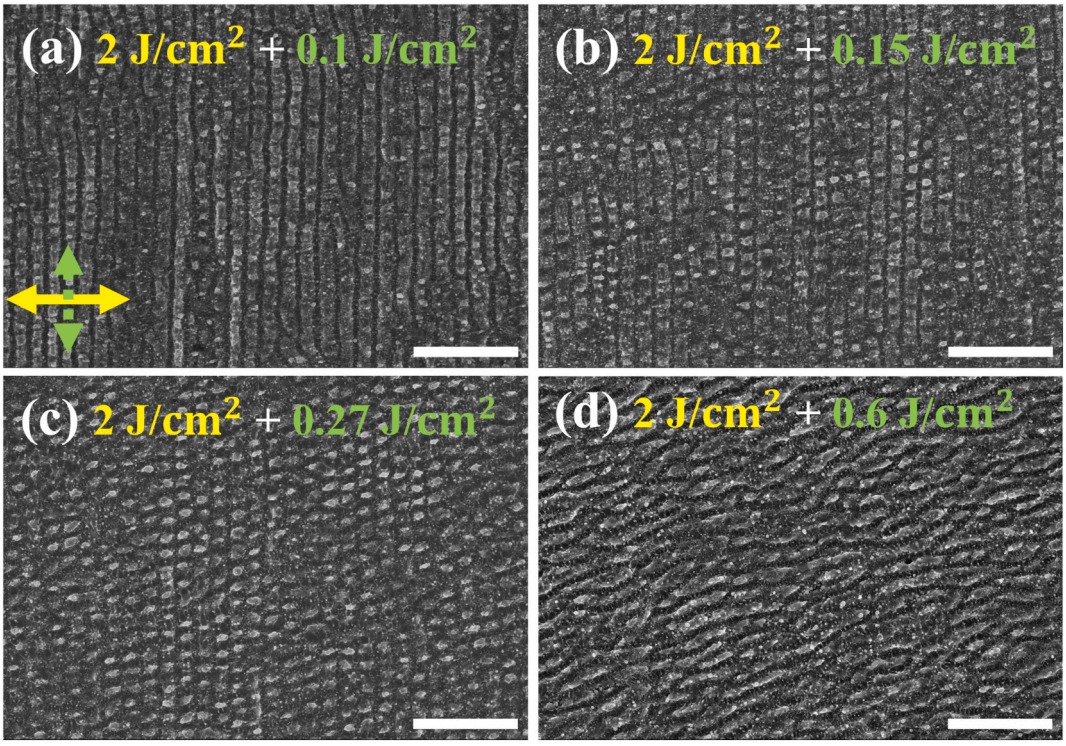

Fig. 5. Nanobump formation behavior with respect to laser fluence of the second scan. The laser fluences of the first (second) scan are marked in yellow (green). The yellow (green) double arrow indicates the polarization direction of the first (second) scan. The overlapping ratios of both scans are set at 75 %. The scale bar is 5 μm. (For interpretation of the references to color in this figure legend, the reader is referred to the web version of this article.)

the nanoripples are identical to those created by the first scan alone, indicating that 0.1 J/cm^2 is insufficient for nanoripple formation by the second scan. When laser fluence is raised to 0.15 J/cm^2, visible discontinuity takes place on the nanoripples created by the first scan. This means nanoripple formation by the second scan is now effective. With 0.27 J/cm^2, uniform formation of nanobumps are observed, reflecting that the laser energy in the second scan is effective at forming new nanoripples as well as sustaining pre-existing nanoripples. Once the laser pulse energy becomes too strong, such as 0.6 J/cm^2, however, the structures revert to nanoripples but with an orientation orthogonal to that of the first scan. This indicates that these nanoripples are mainly formed by the second scan, which supersede those formed by the first scan. Therefore, the laser fluence of the second scan must be prudently selected for the generation of nanobumps. The correlation with the laser fluence in the first scan should also be considered.

The overlapping ratio has a substantial effect on nanobump formation as well. Fig. 6 depicts nanobump evolution behavior with varying overlapping ratios in the second scan. Here laser fluences of the first and second scans were 2 J/cm^2 and 0.6 J/cm^2, respectively. The overlapping ratio in the first scan was kept at 75 %. Polarization directions in these two consecutive scans remained orthogonal ($\theta = 90°$). Even with a high laser pulse fluence, a low overlapping ratio (50 % in this instance) is insufficient to activate the production of nanobumps, as shown in Fig. 6 (a). Nanoripples created by the first scan still cover the processed area. When the overlapping ratio increases to 55 %, deposited laser energy becomes strong enough, and nanobumps begin to develop evenly. And they keep forming well with laser pulses more confined along the scanning direction, such as a 70 % overlapping ratio. When the overlapping ratio becomes too high, representing very severe laser energy deposition, pre-generated nanoripples would be taken over by the nanoripples induced through the second scan. Thus, even with a sufficient laser fluence, the overlapping ratio of the second scan must be carefully considered to produce nanobumps.

The structures formed at various laser fluences and overlapping ratios of the second scan are summarized in Fig. 7 with the first scan fluence of 2 J/cm^2, the first scan overlapping ratio of 75 % and the polarization angle of 90°. A broad formation window for nanobumps can be identified (the green square zone). A second scan with laser fluence varying from 0.1 J/cm^2 to 0.8 J/cm^2 is suitable to induce the formation of nanobumps. In general, there is an inverse correlation between laser fluence and overlapping ratio effects over nanobumps formation: a smaller overlapping ratio is preferable when a greater laser fluence is used. This behavior mainly relies on the growth of the second scan-induced nanoripples. The key to achieving nanobumps is creating

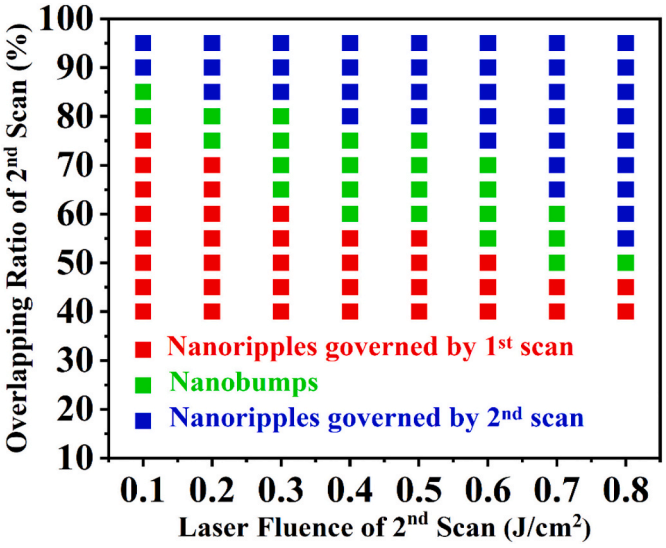

Fig. 7. Nanobump formation window with respect to laser fluence and overlapping ratio of the second scan.

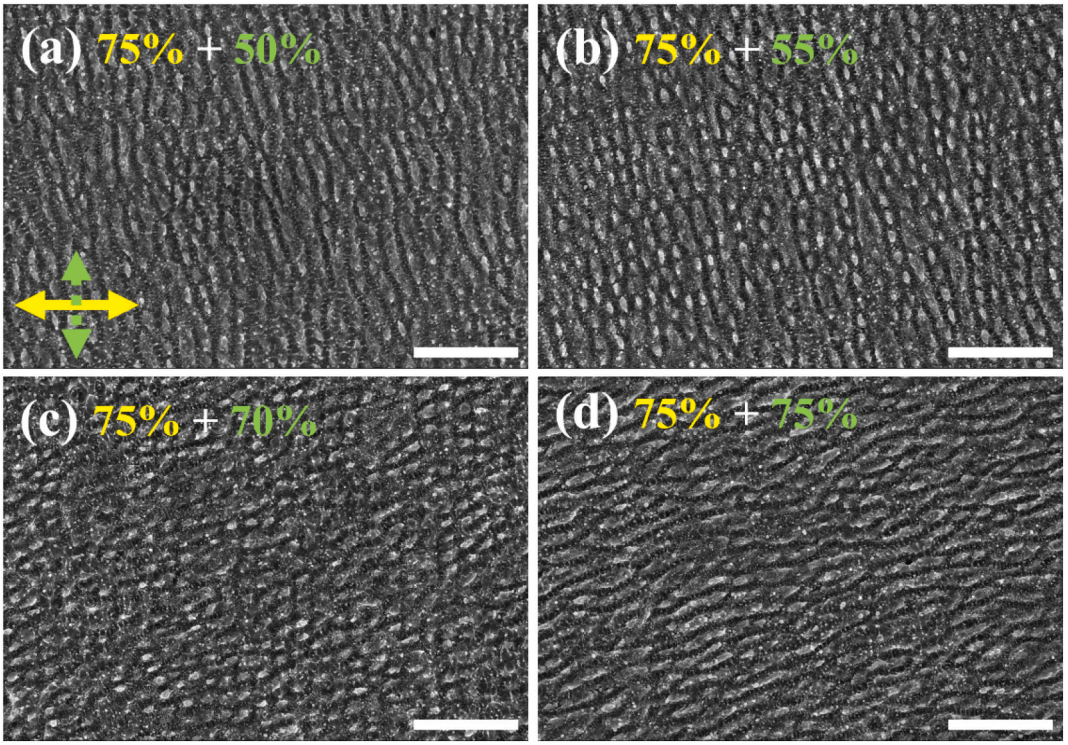

Fig. 6. Nanobump formation behavior with respect to overlapping ratio of the second scan. The overlapping ratios of the first (second) scan are marked in yellow (green). The yellow (green) double arrow indicates the polarization direction of the first (second) scan. The laser fluence of the first (second) scan is set as 2 J/cm^2 (0.6 J/cm^2). The scale bar is 5 μm. (For interpretation of the references to color in this figure legend, the reader is referred to the web version of this article.)

nanoripples by the second scan while preserving the ones generated by the first scan. A high laser fluence paired with a high overlapping ratio will strengthen the formation of the second scan-induced nanoripples and subsequently completely eradicate the nanoripples generated by the first scan. A balance between laser fluence and overlapping ratio is required to keep the second scan-induced nanoripples milder than the first scan-induced nanoripples.

3.3. Effect of the polarization angle

For this double-scan method, the polarization angle between two scans is critical for in-depth analysis and precise control in industrial applications. The effect of different polarization angles (θ) on formation behavior was investigated. The laser fluences of the first and second scans were 2 J/cm^2 and 0.25 J/cm^2, respectively. The overlapping ratio was set at 75 % for both scans. Fig. 8 illustrates the nanobumps formation at different regions affected by various polarization angles. As seen in Fig. 8(a-1), nanoripples are created successfully in certain places and are designated as "normal nanoripples" because they are exactly perpendicular to the polarization direction of the initial scan. In some regions, however, owing to localized instability in the laser absorption process and thermal re-equilibrium process, the production of nanoripples deviates from ideal circumstances and cannot extend precisely along vertical directions, as seen in Fig. 8(a-2); these regions referred to as "abnormal nanoripples." Depending on the polarization angle, nanobumps behave differently in these two locations. A relatively modest polarization angle, such as 50° (Fig. 8(b-1)), is sufficient to initiate the production of nanobumps in regions covered by normal nanoripples. With increasing θ, the second scan is capable of generating uniform nanobumps (Fig. 8(c-1–d-1)). Nonetheless, for the regions covered by abnormal nanoripples, 50° (Fig. 8(b-2)) is too small to initiate the formation of nanobumps. When θ exceeds 60° (Fig. 8(c-2–d-2)), universal nanobumps formation could be observed. Such an interesting phenomenon can actually be understood by checking the local polarization angle. For abnormal nanoripples, the virtual polarization direction of the first scan is already at an angle of tilt. Due to the existence of a slanted angle, the local polarization angle in these places becomes lower when the second scan is performed. Therefore, a greater apparent polarization angle is necessary to compensate for the slanted angle and initiate the creation of nanobumps.

The dimensions of nanobumps were also studied. Based on our hypothesis that nanobumps are achieved through superimposition of two sets of nanoripples, an equation (Eq. (4)) has been proposed to reveal the relationship between periodicity of nanobumps ($d_{nanobumps}$) and nanoripples ($d_{nanoripples}$),

$$d_{nanobumps} = \frac{d_{nanoripples}}{sin\theta}, \tag{4}$$

where $d_{nanobumps}$ is the distance between two consecutive nanobumps along the orientations of nanoripples induced by the first and second scans, and $d_{nanoripples}$ represents the distance between two adjacent nanoripples, as shown in Fig. 9(a). Based on our proposed explanation, $d_{nanobumps}$ should be identical along these two directions. Fig. 9(b) discloses the nanobump spatial feature variation with varying polarization angles. The values predicted by Eq. (4) are plotted as well for comparison. When θ exceeds 60°, well-defined nanobumps could be formed, and the periodicities in both directions are identical as expected. The prediction by Eq. (4) agrees well with the experimental measurements, confirming our theory. When θ is smaller than 50°, only nanoripples are formed within the processed area. Consequently, Eq. (4) is not applicable, and a constant periodicity of around 850 nm, which is the geometry size of LSFLs induced by one scan, is measured for all cases. It is interesting to observe that no nanobump can form at low polarization angles (below 50°). This phenomenon is attributed to nanobump size limit induced by the laser spot size. Theoretically, if nanobumps could be formed at small angles, their size ($d_{nanobumps}$) would be very large, over

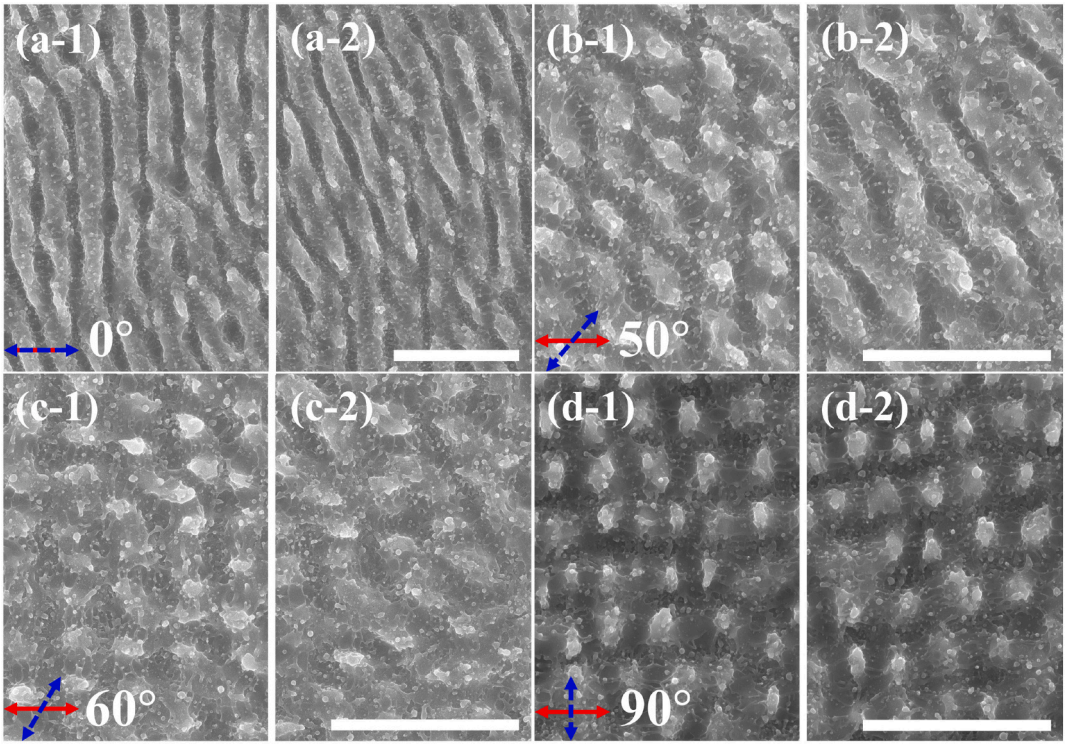

Fig. 8. Nanobump formation at different regions. (a-1), (b-1), (c-1) and (d-1): normal nanoripples region with $\theta = 0°$, 50°, 60° and 90°; (a-2), (b-2), (c-2) and (d-2): abnormal nanoripples region with $\theta = 0°$, 50°, 60° and 90°. The red (blue) double arrow indicates the polarization direction of the first (second) scan. The laser fluence of the first (second) scan is 2 J/cm^2 (0.25 J/cm^2). The overlapping ratios of both scans are 75 %. The scale bar is 3 μm. (For interpretation of the references to color in this figure legend, the reader is referred to the web version of this article.)

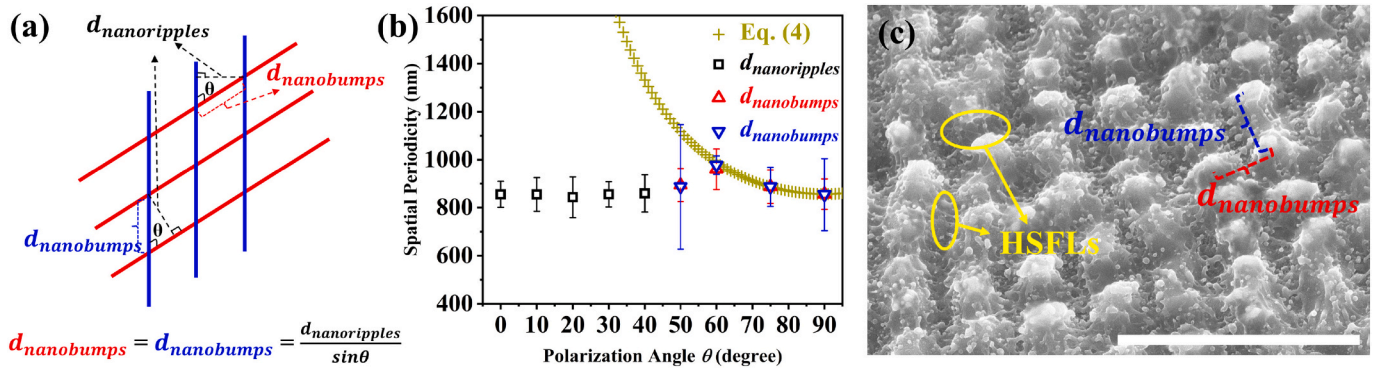

Fig. 9. (a): Correlation between spatial periodicity of nanobumps and nanoripples. Red (blue) lines represent virtual nanoripples induced by the first (second) scan. (b): Spatial periodicity of nanobumps with varying polarization angles. (c): tilted view of nanobumps ($\theta = 90°$). Laser fluence of first (second) scan is 2 J/cm^2 (0.25 J/cm^2). The overlapping ratio is 75 %. The scale bar is 3 μm. (For interpretation of the references to color in this figure legend, the reader is referred to the web version of this article.)

tens of micrometers, according to Eq. (4) (Fig. 9(b)). This dimension is already beyond the size of the effective laser spot, where the local intensity exceeds the ablation threshold. Therefore, nanobump formation will not occur because it lies outside of the ablation region. In addition, such periods that are too great are more susceptible to local thermal instability and will be overwritten by local fluctuations in the flow of molten material. As a result, when θ is small, no formation of nanobumps could be observed. When θ gets close to 50°, $d_{nanobumps}$ is reduced to an adequate level that the superimposition behavior of the second scan-induced nanoripples becomes observable and the formation of nanobumps takes place. Moreover, the tilted view of nanobumps in Fig. 9(c) discloses that each generated nanobump is surrounded by HSFLs with orthogonal directions. Such isotropic HSFLs represent the effects of the superposition of nanoripples in the double-scan method, which further supports our hypothesis.

3.4. Discussion on the formation mechanism

As mentioned previously, several groups reported the successful creation of periodic nanobumps through either the double-pulse method or the double-scan method. But the formation mechanism is still under debate.

First, it is worth mentioning that the formation mechanism of nanobumps in the double-scan method is different from that in the double-pulse method. In the latter method, the interpulse delay is primarily set around the picosecond or nanosecond level where the material surface is still out of the thermal equilibrium state. Under such conditions, strong material excitation induced by the second pulse and regulated molten material flow on the surface are considered the driving force of triangular nanostructure formation. In contrast, the double-scan method uses a pulse interval greater than microseconds, and the material has already returned to a condition of thermal equilibrium. Therefore, from the perspective of the excitation state of the material, laser pulses from the second scan in the double-scan method are delivered to unexcited material, while (the second) laser pulses are fired on a highly excited material surface in the double-pulse method.

Secondly, for the double-scan method, different mechanisms were proposed for nanobump formation, including dynamic self-organization [23], surface reconstruction [24], and the cutting effect of HSFLs induced by the second scan [26]. However, we observed experimental results contradicting these proposed hypotheses. The observation that nanobump formation is dependent on polarization angles demonstrates the predominance of laser polarization and diminishes the plausibility of the dynamic self-organization explanation. The spatial periodicities of nanobumps in both directions are found close to those of LSFLs, excluding the cutting effect from HSFLs induced by the second scan. In addition, HSFLs induced by the second scan, as illustrated in Fig. 9(c), are mainly generated below the nanobumps as opposed to above them, further confirming this conclusion. Physically, after being subjected to the first scan, the reflectivity of the treated region would drop significantly, lowering the effective ablation threshold for the second scan. Consequently, even with a much weaker laser fluence, the second scan is still strong enough to initiate the formation of LSFLs rather than only HSFLs. Moreover, the presence of nanoparticles within the processed area (Figs. 4(c) and 9(c)) clearly shows the occurrence of laser ablation, which contradicts the non-ablative surface reconstruction theory.

We propose, based on our experimental findings, that nanobumps are generated by the superposition of two sets of nanoripples with different orientations that are generated by two consecutive scans. First, the orientation of laser-induced nanoripples is determined solely by the polarization direction and not by the surface morphology. The orientation of the nanoripples generated by the second scan is therefore controllable. Second, the nanoripple formation is the result of ablation, and hence the structures are capable of superposition. Under proper conditions, the nanoripples generated by the second scan will partially etch the first scan-induced nanoripples, forming discrete nanobump structures.

4. Conclusion

In this paper, the formation of periodic nanobumps using a double-scan method is investigated. It is confirmed that the formation of nanobumps is caused by the superposition of two sets of nanoripples (LSFLs) induced by two successive scans. The key to the fabrication of these periodic nanostructures is the careful selection of the second scan parameters. When the laser fluence or overlapping ratio is insufficient, the obtained structures will be the nanoripples formed by the first scan. At excessive fluences or overlapping ratios, the structures will be dominated by the nanoripples created by the second scan. Nanobumps can only be obtained with moderate fluences and overlapping ratios. Also crucial is the polarization angle between two scans. The formation of nanobumps can be induced by polarization angles ranging from 50° to 90°. With a significantly larger effective viewing angle, the obtained nanobumps exhibits much better surface coloration effects compared to commonly employed nanoripples. This simple double-scan method greatly expands the potential applications of ultrafast laser surface structuring for surface color regulation. In addition, the capability on regulating isotropic spatial periodicity brought from this method could be beneficial for developing hydrophobic/hydrophilic surfaces for surface wettability-related applications such as anti-fouling, anti-fogging and anti-icing.

Declaration of competing interest

The authors declare that they have no known competing financial interests or personal relationships that could have appeared to influence the work reported in this paper.

Acknowledgements

The authors would like to gratefully acknowledge the financial support provided for this study by the National Science Foundation (Grant No: 2047000-CMMI). The authors thank Clemson University Electron Microscopy Facility for the access to scanning electron microscopy.

References

[1] Smith GS. Structural color of morpho butterflies. Am J Phys 2009;77:1010–9. https://doi.org/10.1119/1.3192768.
[2] Lee HJ, Michielsen S. Lotus effect: superhydrophobicity. J Text Inst 2006;97:455–62. https://doi.org/10.1533/joti.2006.0271.
[3] Ahmmed K, Grambow C, Kietzig A-M. Fabrication of micro/nano structures on metals by femtosecond laser micromachining. Micromachines 2014;5:1219–53. https://doi.org/10.3390/mi5041219.
[4] Gattass RR, Mazur E. Femtosecond laser micromachining in transparent materials. Nat Photonics 2008;2:219–25. https://doi.org/10.1038/nphoton.2008.47.
[5] Li K, Zhao X. Formation of micro-/nano-surface structures on stainless steel by ultrafast lasers. Vol. 2 Process. mater. American Society of Mechanical Engineers; 2019. https://doi.org/10.1115/MSEC2019-3023.
[6] Zhang Y, Jiao Y, Li C, Chen C, Li J, Hu Y, et al. Bioinspired micro/nanostructured surfaces prepared by femtosecond laser direct writing for multi-functional applications. Int J Extrem Manuf 2020;2:032002. https://doi.org/10.1088/2631-7990/ab95f6.
[7] Lei S, Zhao X, Yu X, Hu A, Vukelic S, Jun MBG, et al. Ultrafast laser applications in manufacturing processes: a state-of-the-art review. J Manuf Sci Eng 2020:142. https://doi.org/10.1115/1.4045969.
[8] Wu J, Yin K, Xiao S, Wu Z, Zhu Z, Duan J-A, et al. Laser fabrication of bioinspired gradient surfaces for wettability applications. Adv Mater Interfaces 2021;8:2001610. https://doi.org/10.1002/admi.202001610.
[9] Wu B, Zhou M, Li J, Ye X, Li G, Cai L. Superhydrophobic surfaces fabricated by microstructuring of stainless steel using a femtosecond laser. Appl Surf Sci 2009;256:61–6. https://doi.org/10.1016/j.apsusc.2009.07.061.
[10] Li K, Myers N, Bishop G, Li Y, Zhao X. Study of surface wettability on fused silica by ultrafast laser-induced micro/nano-surface structures. J Manuf Process 2022;79:177–84. https://doi.org/10.1016/j.jmapro.2022.04.035.
[11] Zhao Y, Xie Z, Gu H, Zhu C, Gu Z. Bio-inspired variable structural color materials. Chem Soc Rev 2012;41:3297. https://doi.org/10.1039/c2cs15267c.
[12] Wu P, Cao X, Zhao L, Chen Z, Zhang M, Juodkazis S, et al. Dynamic structural color display based on femtosecond laser variable polarization processing. Adv Mater Interfaces 2021;8:2100460. https://doi.org/10.1002/admi.202100460.
[13] Zhang D, Ranjan B, Tanaka T, Sugioka K. Underwater persistent bubble-assisted femtosecond laser ablation for hierarchical micro/nanostructuring. Int J Extrem Manuf 2020;2:015001. https://doi.org/10.1088/2631-7990/ab729f.
[14] Müller F, Kunz C, Gräf S. Bio-inspired functional surfaces based on laser-induced periodic surface structures. Materials (Basel) 2016;9:476. https://doi.org/10.3390/ma9060476.
[15] Bonse J, Koter R, Hartelt M, Spaltmann D, Pentzien S, Höhm S, et al. Tribological performance of femtosecond laser-induced periodic surface structures on titanium and a high toughness bearing steel. Appl Surf Sci 2015;336:21–7. https://doi.org/10.1016/j.apsusc.2014.08.111.
[16] Fraggelakis F, Mincuzzi G, Lopez J, Manek-Hönninger I, Kling R. Controlling 2D laser nano structuring over large area with double femtosecond pulses. Appl Surf Sci 2019;470:677–86. https://doi.org/10.1016/j.apsusc.2018.11.106.
[17] Qiao H, Yang J, Li J, Liu Q, Liu J, Guo C. Formation of subwavelength periodic triangular arrays on tungsten through double-pulsed femtosecond laser irradiation. Materials (Basel) 2018;11:2380. https://doi.org/10.3390/ma11122380.
[18] Jalil SA, Yang J, ElKabbash M, Cong C, Guo C. Formation of controllable 1D and 2D periodic surface structures on cobalt by femtosecond double pulse laser irradiation. Appl Phys Lett 2019;115:031601. https://doi.org/10.1063/1.5103216.
[19] Makin VS, Pestov YI, Makin RS. The mechanism of formation of nanostructures of hexagonal symmetry on surfaces of metals by a sequence of doubled ultrashort pulses of radiation of orthogonal polarization. Opt Spectrosc 2020;128:264–8. https://doi.org/10.1134/S0030400X20020149.
[20] Wang S, Jiang L, Han W, Liu W, Hu J, Wang S, et al. Controllable formation of laser-induced periodic surface structures on ZnO film by temporally shaped femtosecond laser scanning. Opt Lett 2020;45:2411. https://doi.org/10.1364/OL.388770.
[21] Mastellone M, Bellucci A, Girolami M, Serpente V, Polini R, Orlando S, et al. Deep-subwavelength 2D periodic surface nanostructures on diamond by double-pulse femtosecond laser irradiation. Nano Lett 2021;21:4477–83. https://doi.org/10.1021/acs.nanolett.1c01310.
[22] Limaye SV. Study of ultrafast laser-induced surface structures on stainless steel and fused silica for optical property modification. United States – South Carolina: Clemson University PP; 2020.
[23] Gregorčič P, Sedlaček M, Podgornik B, Reif J. Formation of laser-induced periodic surface structures (LIPSS) on tool steel by multiple picosecond laser pulses of different polarizations. Appl Surf Sci 2016;387:698–706. https://doi.org/10.1016/j.apsusc.2016.06.174.
[24] Kobayashi T, Yan J. Generating nanodot structures on stainless-steel surfaces by cross scanning of a picosecond pulsed laser. Nanomanufacturing Metrol 2020;3:105–11. https://doi.org/10.1007/s41871-020-00063-6.
[25] Hermens U, Pothen M, Winands K, Arntz K, Klocke F. Automated polarization control for the precise alignment of laser-induced self-organized nanostructures. Opt Lasers Eng 2018;101:44–50. https://doi.org/10.1016/j.optlaseng.2017.10.001.
[26] Liu Y-H, Yeh S-C, Cheng C-W. Two-dimensional periodic nanostructure fabricated on titanium by femtosecond green laser. Nanomaterials 2020;10:1820. https://doi.org/10.3390/nano10091820.
[27] Chen L, Zhang Y, Kodama S, Xu S, Shimada K, Mizutani M, et al. Picosecond laser-induced nanopillar coverage of entire mirror-polished surfaces of Ti6Al4V alloy. Precis Eng 2021;72:556–67. https://doi.org/10.1016/j.precisioneng.2021.07.004.
[28] Http://gwyddion.net/.
[29] Li G, Li J, Hu Y, Zhang C, Li X, Chu J, et al. Femtosecond laser color marking stainless steel surface with different wavelengths. Appl Phys A 2015;118:1189–96. https://doi.org/10.1007/s00339-014-8868-3.